ARTICLE

Check for updates

A macroscopic mass from quantum mechanics in an integrated approach

Frank C. Seifert[1,2], Alireza R. Panna[1], I-Fan Hu [1,3], Lorenz H. Keck [1], Leon S. Chao[1], Shamith U. Payagala[1], Dean G. Jarrett [1], Chieh-I Liu[1,4], Dipanjan Saha[1], Randolph E. Elmquist [1], Stephan Schlamminger [1], Albert F. Rigosi [1], David B. Newell[1] & Darine Haddad [1✉]

The revision of the International System of Units (SI) on May 20th, 2019, has enabled new improved experiments to consolidate and simplify mechanical and quantum electrical metrology. Here, we present the direct measurement between a macroscopic mass and two quantum standards in a single experiment, in which the current used to levitate a mass passes through a graphene quantum Hall standard. The Josephson effect voltage is compared directly to the resulting quantum Hall effect voltage. We demonstrate this measurement with the use of graphene quantum Hall arrays for scaling in resistance with improved uncertainty and higher current level.

[1] National Institute of Standards and Technology (NIST), 100 Bureau Drive Stop 8171, Gaithersburg, MD 20899, USA. [2] University of Maryland, Joint Quantum Institute, College Park, MD 20742, USA. [3] Department of Physics, National Taiwan University, Taipei 10617, Taiwan. [4] Department of Chemistry and Biochemistry, University of Maryland, College Park, MD 20742, USA. ✉email: darine.haddad@nist.gov

Historically within the SI, the definition of energy was only available in the mechanical realm where the units of mass, time, and length were given. Consequently, electrical units could only be defined via complicated mechanical experiments. Previously, the ampere was defined as the current flowing between two parallel wires producing a well defined force between them, an abstraction that was difficult to realize experimentally. With the advent of quantum electrical standards, specifically the prediction of the Josephson effect by B. Josephson in 1962[1], and the discovery of the quantum Hall effect by K.v. Klitzing in 1980[2], the mechanical realization of electrical units ceased, and electrical units became disjointed from the SI, and were used as "conventional" units internationally. The revision in 2019 removed this dichotomy and consolidated our system of units. The mechanical unit of mass is defined via electrical power using the Josephson and the quantum Hall effect. While the Kibble balance[3] has successfully rationalized the unit of mass, the kilogram, it has never done so in a single experimental setup. Typically, the von Klitzing constant is realized in a separate experiment and used in the Kibble balance via a traditional transfer standard, a wire or thin film resistor. Researchers at the National Institute of Standards and Technology (NIST) employed two quantum electrical standards in a single current source arrangement with the coil of a Kibble balance to levitate a mass as shown in Fig. 1.

Results

Quantization of graphene quantum Hall standards. Quantum Hall array resistance standards (QHARS) have been explored in the recent past, but were limited in the amount of current that
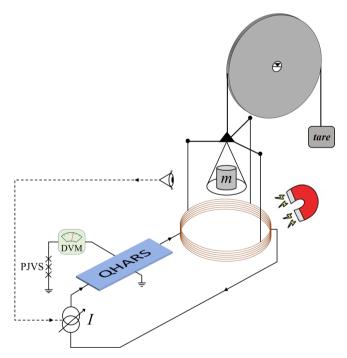
could pass through the device before quantization breaks down[4–7]. At NIST, we developed SiC-graphene standards with thirteen quantum Hall arrays in parallel giving an equivalent resistance of $R_K/26$, where R_K is the von Klitzing constant, defined by $R_K = h/(e^2)$. The elementary charge e and the Planck constant h are now defined in the SI as exact; They are two of the seven defining constants of the SI. Magnetic field reversal measurements were used to test quantization for QHARS devices since the absence of longitudinal dissipation cannot be experimentally confirmed for each element of the array. Figure 2 shows the Hall resistance and the magnetic field reversal measurements as a function of source-drain current for the QHARS devices. For the results shown in Fig. 2, four QHARS devices (QHARS1-D1, QHARS1-D2, QHARS2-D1, and QHARS2-D2) were used. The devices were immersed in a liquid ^{4}He reservoir maintained at temperature $T = 1.6$ K. A cryogenic current comparator bridge was used along with multiple $100\,\Omega$ standards to measure the Hall resistance as a function of the source-drain current as shown in Fig. 2. The $100\,\Omega$ standards that were used to characterize these QHARS devices are measured periodically against a GaAs quantum Hall resistance standard at NIST. Table 1 shows the deviation from $R_K/26$ for the four quantum Hall arrays along with their dispersion. All devices showed quantization at $|B| = 9$ T, and magnetic field reversal measurements confirmed quantization. The apparent higher deviation seen in Fig. 2 for the device QHARS2-D1 when measured at 0.1 mA can be explained by the higher type A standard uncertainty of $\approx 7\,n\Omega/\Omega$ for this measurement. Since artifact resistance standards were used to confirm the quantization of the arrays, the non-zero group average of $(-2.72 \pm 0.31) \times 10^{-9}$ can be attributed to the stability of the standards, leakage errors in the insulation of the cables, and the cryogenic current comparator's balance electronics.

Mass measurements. Though historically it was common to calibrate masses using a 1 kg artifact, the revised SI allows for the possibility of calibrating any mass value directly. This enabled us to do a primary measurement of 50 g and 100 g masses with results yielding relative uncertainties $(k = 1)$ on the order of 3×10^{-8}. In the measurements shown in Fig. 3, each mass is placed on the Kibble balance mass pan, and the experiment is evacuated to a base pressure in the order of 10^{-4} Pa. All four QHARS devices were used and alternated with air or oil standard resistors with nominal values of $100\,\Omega$ and $1000\,\Omega$. The standard resistors were calibrated against the GaAs quantum Hall standard and were chosen for their low-temperature coefficients and power coefficients. The temporal drift coefficient along with the temperature and power coefficients for these standard resistors are shown in Table 2. A drift correction was applied for the mass measurement with the standard resistors. The vacuum was interrupted once during the 100 g mass measurement due to an emergency outage in the laboratory. This caused a larger drift in the Kibble balance experiment, producing a larger scatter in the QHARS1-D1 and the $100\,\Omega$ in oil measurements. Otherwise, the only change to the experimental setup was the connection to either quantum or traditional resistors in the electrical circuit. The deviation in the mass value between QHARS devices and traditional resistors is $(-21.5 \pm 12.8) \times 10^{-9}$ for the 100 g mass, and $(-2.6 \pm 20) \times 10^{-9}$ for the 50 g mass as reflected in the histogram of Fig. 3. The deviation is larger with the 100 g mass due to a resistance leakage problem discovered with the $1000\,\Omega$ standard oil resistor after the measurement campaign ended. By omitting the $1000\,\Omega$ standard oil resistor data, the deviation between QHARS devices and traditional resistor is reduced to $(-3.7 \pm 14.4) \times 10^{-9}$ for the 100 g mass.
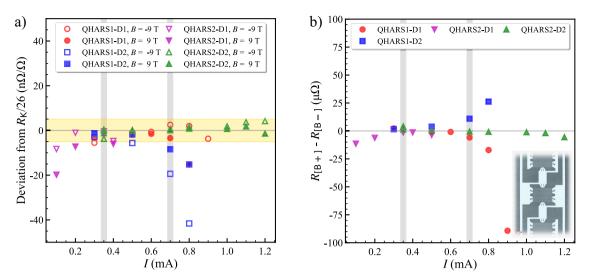

Fig. 1 A macroscopic mass from two quantum effects. The quantum Hall voltage resulting from passing current I through a graphene quantum Hall array resistance standard (QHARS) device is monitored with respect to the programmable Josephson voltage standard (PJVS). The current I is injected directly into the Kibble balance coil to provide an electromagnetic force (see Fig. 5 for details) to counter the mechanical force of a standard macroscopic mass m in gravity. The position of the balance is monitored and maintained level by providing small changes to the current I. The PJVS is adjusted until the voltage measured is almost zero to achieve the lowest uncertainty.

Fig. 2 Verification of quantization of quantum Hall array standards. Cryogenic current comparator bridge measurements for four quantum Hall array resistance standards (QHARS), (QHARS1-D1, QHARS1-D2, QHARS2-D1, and QHARS2-D2) at $T = 1.6$ K and $|B| = 9$ T. **a** The deviation of the measured resistance of QHARS devices from the nominal value of $R_K/26$ as a function of source-drain current[38, 39]. The QHARS devices were used at 0.35 mA and 0.7 mA (gray bands) to measure 50 g and 100 g masses where they showed excellent quantization. **b** The magnetic field reversal measurements for the four QHARS devices as a function of source-drain current. Inset: layout of indvidual graphene quantum elements in the QHARS devices.

Table 1 Weighted averages of the quantum Hall array resistance standards (QHARS) in the pre-breakdown regime.

Array	I (mA)	Dev. from $R_K/26$ (nΩ/Ω)	Std. Unc. $k = 1$, (nΩ/Ω)
QHARS1-D1	$0.3 \le I \le 0.7$	−1.78	0.29
QHARS1-D2	$0.3 \le I \le 0.7$	−6.00	0.51
QHARS2-D1	$0.3 \le I \le 0.4$	0.12	0.28
QHARS2-D2	$0.3 \le I \le 0.7$	−3.19	1.00

Discussion

The ampere has always demonstrated a subtle difficulty in measurement, except when derived from the Josephson and quantum Hall effect. This unit has been realized with single-electron transistors[8–12], and more recently in ref. [13], which provide the benefit of direct connection to the ampere when linked with a frequency standard. So far, these devices can only provide currents in the nanoampere range, rendering them less practical for many experimental applications. Here, the Kibble balance and the quantum electrical standards validate the use of virtual quantum current sources many orders of magnitude larger, directly traceable to the revised SI. The current being applied is determined quantum mechanically via the current-to-voltage conversion with the graphene QHARS and the determination of the converted voltage with the programmable Josephson voltage standard (PJVS). The order of magnitude of current that is now accessible by this experimental setup places the quantum ampere within reach of global democratization of standards.

Figure 4 shows the metrology triangle involving the Kibble balance, the Josephson effect, and the quantized Hall effect, showing the scaled connections to the defining constants of the SI. The triangle is analogous to the original quantum electrical metrology triangle[14] with the single-electron tunneling effect for current being replaced by a Kibble balance.

The closure of the metrology triangle involves the comparison of two measurements of the same quantity from the two directions around the triangle. As of this writing, international mass
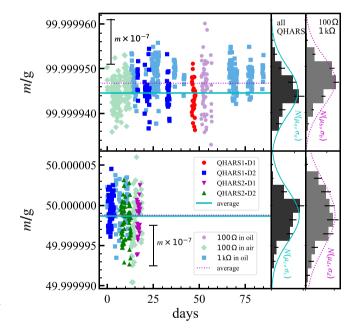

Fig. 3 Primary realization of a 100 g and a 50 g stainless steel masses. For each mass measurement, the resistor R in the circuit was changed to be different 100 Ω and 1000 Ω standard oil or air resistors, as well as different quantum Hall array resistance standards (QHARS).

dissemination is presently through the international consensus value of the kilogram, which includes data directly traceable to the International Prototype of the kilogram, data from the 2016 Consultative Committee on Mass and related Quantities Pilot Study of realization experiments involving three Kibble balances and two X-Ray Crystal Density (XRCD) primary realizations, and the key comparison CCM.M-K8.2019 on realizations of the kilogram involving four Kibble balances, one Joule balance, and two XRCD results [15]. There is a small correlation between the measurement reported here and the consensus value because a data point from NIST-4 has been used to establish the consensus value. The relative weight of the NIST-4 measurement to the

Table 2 Technical data of the standard resistors used in the experiment.					
Value [Ω]	Bath	Temp. [°C]	Rel. drift $[(n\Omega/\Omega)/yr]$	Temp. coeff. $[(n\Omega/\Omega)/K]$	Pwr. coeff. $[(n\Omega/\Omega)/mW]$
100	Air	23	7.3	−40	0.5
100	Oil	25	32	−78	0.6
1000	Oil	25	43.5	−9.9	8.1

Fig. 4 The metrology triangle. The metrology triangle involving the Kibble balance (KB), and two quantum standards : the programmable Josephson voltage standard (PJVS), and the Quantum Hall array resistance standards (QHARS). For the measurement presented here, the nominal values of the scaling factors for the 100 g mass are $k_R = 1/26$, $k_U = 18,350$, and $k_I = 477,100$.

consensus value is less than 4%. That small relative contribution is further diluted because the contributing measurement was performed at the 1 kg level and with standard resistors. In principle, the metrology triangle can be closed by comparing the measured mass in this study to the international consensus value. In practice, the traditional scaling from Pt-Ir 1 kg mass standards traceable to the consensus value to the stainless steel mass standards used in this study would be the limiting uncertainty. In the future when the kilogram is only directly realized in terms of the Planck constant, the closure of the metrology triangle can be achieved through the comparison of a mass from a Kibble balance and an independent method that does not involve the quantum electrical standards, such as the XRCD method.

Conclusion

With the redefinition of the SI, mass artifacts in the laboratory are referenced against invariable electrical standards using a Kibble balance. By incorporating the fundamental quantum standards of voltage and resistance in the Kibble balance, as this work demonstrates for the levels of 50 g and 100 g, we show how artifact resistance standards also can be gradually removed from the measurement chain, thus focusing on absolute standards in all phases of calibration.

Methods

The three major components used in the experimental setup were designed and built at NIST: the programmable Josephson voltage standard, the graphene quantum Hall array standard, and the Kibble balance.

Programmable Josephson voltage standard. A Josephson junction is a frequency to voltage converter, converting a microwave reference frequency to a dc voltage standard[16]. The potential difference between two superconductors separated by a thin insulating barrier in the presence of a bias current at frequency v is given by $K_J^{-1}v$, where K_J is the Josephson constant defined by $K_J = 2e/h$. The frequency v can be expressed as a scaling factor k_v of the hyperfine transition frequency of ^{133}Cs (another one of the seven defining constants),

$$v = k_v \Delta v_{Cs}. \tag{1}$$

By using n junctions in series, a larger voltage

$$U = k_U k_v \Delta v_{Cs} \frac{h}{e} \text{ with } k_U = \frac{n}{2} \tag{2}$$

can be obtained. For the measurements shown in this paper, we used a PJVS system designed and built by NIST[17–19] that contains a total of 67406 junctions subdivided into smaller, individually programmable array segments following a ternary sequence for the number of junctions, which are operated at a nominal frequency v of 18.2 GHz. This sequence in combination with small adjustments of the nominal frequency (±10 MHz) allows the realization of voltage up to 2.5 V with an uncertainty of a few nanovolts.

Graphene quantum Hall array standard. The quantum Hall effect arises when a two dimensional (2-D) charge carrying system is cooled down to temperatures typically below 4 K and immersed in a magnetic field perpendicular to the 2-D plane, resulting in the Hall resistance R_H (Hall voltage divided by the applied current) exhibiting well defined constant values $R_H = h/(ie^2) = R_K/i$, where i is the Landau level filling factor.

Epitaxially grown graphene is well established as the successor to GaAs-based quantum Hall resistance standards, demonstrating an exceptionally stable and robust $i = 2$ level at much higher currents and temperatures, and much lower magnetic flux densities[20–22]. High quality epitaxial graphene (EG) was grown at NIST via the thermal decomposition of the Si face of 4H-SiC(0001), in a graphite-lined resistive-element furnace heated to 1900 °C in an argon environment at atmospheric pressure, and using a polymer-assisted sublimation growth technique[23,24]. After growth, the graphene quality was assessed using a confocal laser scanning microscope, which can rapidly identify successful large-area growths[25]. The fabrication steps that followed allow for contaminent free graphene to metal contacting by protecting the epitaxial graphene with a thin layer of Pd/Au followed by Ar plasma etching to structure it in a Hall bar geometry and finally electrically contacting the EG/Pd/Au layer. Notable improvements in the design of these arrays include the use of NbTiN as superconducting electrical contacts[26–28], functionalization with Cr(CO)$_3$ to both homogenize and control the carrier density across the entire device[29], and the implementation of the Delahaye multiple-series interconnections using a split contact geometry[30]. With these improvements, robust quantization is possible with higher currents. The NIST SiC-graphene standards with j quantum Hall arrays in parallel gives a combined resistance of

$$R = k_R \frac{h}{e^2} \text{ with } k_R = \frac{1}{ij}. \tag{3}$$

In our system, $i = 2$ and $j = 13$ giving $R = (h/e^2)/26$. Note that the 13 individual graphene quantum Hall elements in parallel for resistance scaling is a choice we used here, however, other series and parallel combinations are possible[31], including the use of pn junctions within the graphene channel for intrinsic resistance scaling[32]. Thirteen graphene quantum Hall elements in parallel produces a quantum Hall standard with a nominal value close to 1000 Ω. This has the advantage of direct scaling to other decade levels using a room-temperature direct current comparator in a 10:1 ratio. Commercial direct current comparators are designed to have best performance at a 10:1 ratio, so the arrays were designed to accommodate this parameter.

NIST Kibble balance. The Kibble balance is an experiment that uses the principle of Maxwell's equation and the symmetry between Lorentz's force and Faraday's induction, i.e., the coupling factor between force and current in a motor is the same as the one between voltage and velocity in a generator of the same geometry. The device was named after the late Bryan Kibble[33] who published this insight that significantly changed the field of fundamental electrical metrology, and now provides the basis for mass metrology.

There are two modes in this experiment. In the force mode, a mechanical balance is used to compare an electromagnetic force produced by a coil in a
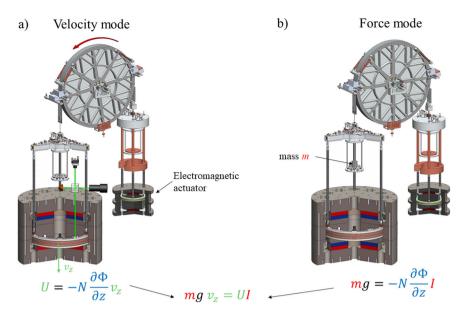
a) Velocity mode   b) Force mode

$$U = -N \frac{\partial \Phi}{\partial z} v_z,$$
$$mg\, v_z = UI$$
$$mg = -N \frac{\partial \Phi}{\partial z} I$$

Fig. 5 NIST Kibble balance with a wheel for the central mechanism. a In the velocity mode, an electromagnetic actuator rotates the wheel and hence the coil moves vertically through the magnetic field. An induced voltage U across the coil is generated, which is proportional to the product of the vertical velocity v_z, the number of turns N and the negative derivative of the flux with respect to z, i.e., $-\partial\Phi/\partial z$. **b** In the force mode, the electromagnetic force $-N\partial\Phi/\partial z I$ is generated by the coil carrying current I placed in the same magnetic field.

magnetic field to the weight of a test mass, i.e.,

$$mg = -N \frac{\partial \Phi}{\partial z} I, \tag{4}$$

where m is the mass of a test mass, g is the local gravitational acceleration, I is the current in the coil, N is the number of turns of the wire, and Φ is the magnetic flux linkage to the coil.

Kibble proposed the velocity mode to determine the product of the number of turns and the vertical derivative of the magnetic flux by measuring the induced voltage U and the vertical velocity v_z when the coil is moved vertically in the same magnetic field,

$$-N \frac{\partial \Phi}{\partial z} = \frac{U}{v_z}. \tag{5}$$

The derivative of the flux with respect to z is eliminated by combining Eqs. (4) and (5) together leading to

$$mgv_z = UI, \tag{6}$$

which describes an equivalence between virtual mechanical and electrical power as shown in Fig. 5. The power is considered virtual because voltage and current, as well as weight and velocity, are measured in two separate phases and not simultaneously.

The weighing current I is determined accurately by passing it through a resistor with resistance R and measuring the potential difference U across this resistor. Eq. (6) can now be expressed as

$$mgv_z = \frac{U^2}{R}. \tag{7}$$

To simplify equations and without loss of generality, the potential difference across the resistor was chosen to be equal to the induced voltage in the velocity mode. This condition is not necessary and has not been met for the measurements reported below.

Replacing U and R in Eq. (7) with the expressions from the Josephson effect (twice) and the quantum Hall effect yields

$$mgv_z = \frac{k_U{}^2 k_\nu{}^2 \frac{h^2}{e^2} \Delta\nu_{Cs}^2}{k_R \frac{h}{e^2}} = \frac{k_U{}^2 k_\nu{}^2}{k_R} h\Delta\nu_{Cs}^2. \tag{8}$$

Conveniently, the elementary charge cancels. A relation between a macroscopic mass and the Planck constant is established.

Combining Eqs. (1), (2), (6) and (8), the current from a Kibble balance written in terms of the frequency ν is

$$I = mgv_z/U = \frac{k_U}{k_R} e\nu = k_I e\nu, \text{ with } k_I = \frac{k_U}{k_R}. \tag{9}$$

The velocity and gravity measurements use primary standards of time and length, that are traceable to the two SI defining constants $\Delta\nu_{Cs}$ and the speed of light c. Hence, the velocity can be written as a scaling factor k_ν of the speed of light,

$\nu = k_\nu c$ and the local acceleration of gravity as a product of a scaling factor k_g, c and $\Delta\nu_{Cs}$, such that $g = k_g c \Delta\nu_{Cs}$.

Replacing the quantities v_z and g in Eq. (8) with the above expressions, and summarizing the scaling factors into one, i.e., $k_m = k_U{}^2 k_\nu{}^2/(k_R k_g k_\nu)$ yields a form resembling the mass-energy equivalence,

$$mc^2 = k_m h\Delta\nu_{Cs}. \tag{10}$$

The NIST fourth generation Kibble balance (NIST-4)[34] used in the experimental setup is shown in Fig. 5. NIST-4 is the experiment that measured one of the most precise values of the Planck constant[35] that led to the redefinition of the kilogram. The dominating feature in Fig. 5 is the wheel that can rotate by ± 10 degrees about a horizontal axis given by the knife edge. The wheel serves as the support and the weighing mechanism in the force mode and as the guiding mechanism in the velocity mode. The measurement coil is immersed in a radial magnetic field generated by two opposing Sm_2Co_{17} magnet rings that are symmetrically spaced about a midplane[36]. In the force mode, the current I in the coil is adjusted to maintain the position of the wheel to a nominal position, hence the electromagnetic force and the weight of the mass produce a constant force on one side of the wheel, which equals the dead weight on the other side. The current source is an upgraded version of a low noise, 30 bit programmable source[37]. Optical fiber communication controls the current source and batteries are used for the source power to ensure high-resistance isolation to ground. The current noise is less than 100 pA/$\sqrt{\text{Hz}}$ at 1 Hz for a current of 10 mA. The choice of the resistance R in Eq. (7) depends on the design constraints of the Kibble balance. For the NIST-4 Kibble balance, $-N\frac{\partial\Phi}{\partial z} \approx 700$ Tm in Eq. (4). To realize masses at the 50 g and 100 g level requires that the current, I sourced through the QHARS to be 0.35 mA and 0.7 mA, respectively, using the weighing substitution method. Using a QHARS with fewer than four devices in parallel would exceed the maximum voltage of 2.5 V set by the PJVS for the 100 g mass realization. In the velocity mode, the wheel ensures perfect vertical motion of the coil. The velocity is measured by means of heterodyne laser interferometers in a Michelson configuration.

Data availability

The data that support the findings of this study are available from the corresponding author upon reasonable request.

References

1. Josephson, B. D. Possible new effects in superconductive tunneling. *Phys Lett* **1**, 251–253 (1962).

2. Klitzing, K. V., Dorda, G. & Pepper, M. New method for high accuracy determination of the fine-structure constant based on quantised Hall resistance. *Phys. Rev. Lett.* **45**, 494–497 (1980).

3. Robinson, I. A. & Schlamminger, S. The watt or Kibble balance: a technique for implementing the new SI definition of the unit of mass. *Metrologia* **53**, 46–73 (2016).

4. Novikov, S. Mini array of quantum Hall devices based on epitaxial graphene. *J. Appl. Phys.* **119**, https://doi.org/10.1063/1.4948675 (2016).

5. Lartsev, A. et al. A prototype of R_K/200 quantum Hall array resistance standard on epitaxial graphene. *J. Appl. Phys.* **118**, https://doi.org/10.1063/1.4927618 (2015).

6. Oe, T. et al. Development of 1 MΩ quantum Hall array resistance standards, *IEEE Trans. Instrum. Meas.* **66**, https://doi.org/10.1109/CPEM.2008.4574632 (2017).

7. Park, J., Kim, W.-S. & Chae, D.-H. Realization of 5h/e2 with graphene quantum Hall resistance array. *Appl. Phys. Lett.* **116**, https://doi.org/10.1063/1.5139965 (2020).

8. Averin, D. V. & Nazarov, Y. V. *Single Charge Tunneling* (Plenum Press, 1992).

9. Durrani, Z. A. K. *Single-electron Devices and Circuits in Silicon* (Imperial College Press, 2009).

10. Giblin, S. P. et al. Towards a quantum representation of the ampere using single electron pumps. *Nat. Commun.* **3**, 1–6 (2012).

11. Fricke, L. et al. Self-referenced single-electron quantized current source. *Phys. Rev. Lett.* **112**, https://doi.org/10.1103/PhysRevLett.112.226803 (2014).

12. Koppinen, P. J., Stewart, M. D. & Zimmerman, N. M. Fabrication and electrical characterization of fully CMOS-compatible Si single-electron devices. *IEEE Trans. electron devices* **60**, 78–83 (2012).

13. Myung-Ho, B. et al. Precision measurement of single-electron current with quantized Hall array resistance and Josephson voltage, *Metrologia* **57**, https://doi.org/10.1088/1681-7575/abb6cf (2020).

14. Keller, M. W. Current status of the quantum metrology triangle. *Metrologia* **45**, 102–109 (2008).

15. Davidson, S. & Stock, M. Beginning of a new phase of the dissemination of the kilogram. *Metrologia* **58**, 1–4 (2021).

16. Hamilton, C. A. & Benz, S. P. Broadband Josephson voltage standards. *IEEE MTT-S Int. Microw. Symp .* **2**, 853–856 (2001).

17. Hamilton, C. A., Burroughs, C. J. & Benz, S. P. Josephson voltage standard-a review. *IEEE Trans. Appl. superconductivity* **7**, 3756–3761 (1997).

18. Benz, S. P. & Hamilton, C. A. Application of the Josephson effect to voltage metrology. *Proc. IEEE* **92**, 1617–1629 (2004).

19. Rüfenacht, A., Flowers-Jacobs, N. E. & Benz, S. P. Impact of the latest generation of Josephson voltage standards in ac and dc electric metrology. *Metrologia* **55**, S152–S173 (2018).

20. Rigosi, A. F. & Elmquist, R. E. The quantum Hall effect in the era of the new SI. *Semicond. Sci. Tech.* **34**, https://doi.org/10.1088/1361-6641/ab37d3 (2019).

21. Oe, T. et al. Comparison between NIST graphene and AIST GaAs quantized Hall devices. *IEEE Trans. Instrum. Meas.* **69**, 3103–3108 (2019).

22. Payagala, S. U. et al. Comparison betweeN Graphene and GaAs quantized hall devices with a dual probe. *IEEE Trans. Instrum. Meas.* **69**, 9374–9380 (2020).

23. Kruskopf, M. et al. Comeback of epitaxial graphene for electronics: large-area growth of bilayer-free graphene on SiC. *2D Materials* **3**, https://doi.org/10.1088/2053-1583/3/4/041002 (2016).

24. Rigosi, A. F. et al. Graphene devices for tabletop and high-current quantized Hall resistance standards. *IEEE Trans. Instrum. Meas.* **68**, 1870–1878 (2018).

25. Panchal, V. et al. Confocal laser scanning microscopy for rapid optical characterization of graphene. *Commun. Phys.* **1**, 1–7 (2018).

26. Kruskopf, M. et al. Two-terminal and multi-terminal designs for next-generation quantized Hall resistance standards: contact material and geometry. *IEEE Trans. Electron Devices* **66**, 3973–3977 (2019).

27. Kruskopf, M. et al. Next-generation crossover-free quantum Hall arrays with superconducting interconnections. *Metrologia* **56**, https://doi.org/10.1088/1681-7575/ab3ba3 (2019).

28. Panna, A. R. et al. Graphene quantum Hall effect parallel resistance arrays. *Phys. Rev. B* **103**, https://doi.org/10.1103/PhysRevB.103.075408 (2021)

29. Rigosi, A. F. et al. Gateless and reversible carrier density tunability in epitaxial graphene devices functionalized with chromium tricarbonyl. *Carbon* **142**, 468–474 (2019).

30. Delahaye, F. Series and parallel connection of multiterminal quantum Hall-effect devices. *J. Appl. Phys.* **73**, 7914–7920 (1993).

31. Hu, I.-F. et al. Onsager-Casimir frustration from resistance anisotropy in graphene quantum Hall devices. *Phys. Rev. B* **104**, https://doi.org/10.1103/PhysRevB.104.085418 (2021).

32. Hu, J. et al. Towards epitaxial graphene p-n junctions as electrically programmable quantum resistance standards *Nat. Sci. Rep.* **8**, https://doi.org/10.1038/s41598-018-33466-z (2018).

33. Kibble, B. P. A measurement of the gyromagnetic ratio of the proton by the strong field method. *Atom. Masses Fundam. Constants* **5**, 545–551 (1976).

34. Haddad, D. et al. Invited Article: A precise instrument to determine the Planck constant, and the future kilogram. *Rev. Sc. Inst.* **87**, https://doi.org/10.1063/1.4953825 (2016).

35. Haddad, D. et al. Measurement of the Planck constant at the National Institute of Standards and Technology from 2015 to 2017. *Metrologia* **54**, https://doi.org/10.1088/1681-7575/aa7bf2 (2017).

36. Seifert, F. et al. Construction, measurement, shimming, and performance of the NIST-4 magnet system. *IEEE Trans. Inst. Meas.* **63**, https://doi.org/10.1109/TIM.2014.2323138 (2016).

37. Haddad, D., Waltrip, B. & Steiner, R. Low noise programmable current source for the NIST-3 and NIST-4 Watt balance. *Conference on Precision Electromagnetic Measurements*, https://doi.org/10.1109/CPEM.2012.6250939 (2012).

38. Delahaye, F. & Jeckelmann, B. Revised technical guidelines for reliable dc measurements of the quantized Hall resistance. *Metrologia* **40**, 217–223 (2003).

39. Jeckelmann, B. & Jeanneret, B. The quantum Hall effect as an electrical resistance standard. *Rep. Prog. Phys.* **64**, 1603–1655 (2001).

Author contributions

Competing interests

The authors declare no competing interests.

Additional information